Supporting Information

Zhang et al. 10.1073/pnas.1710238114

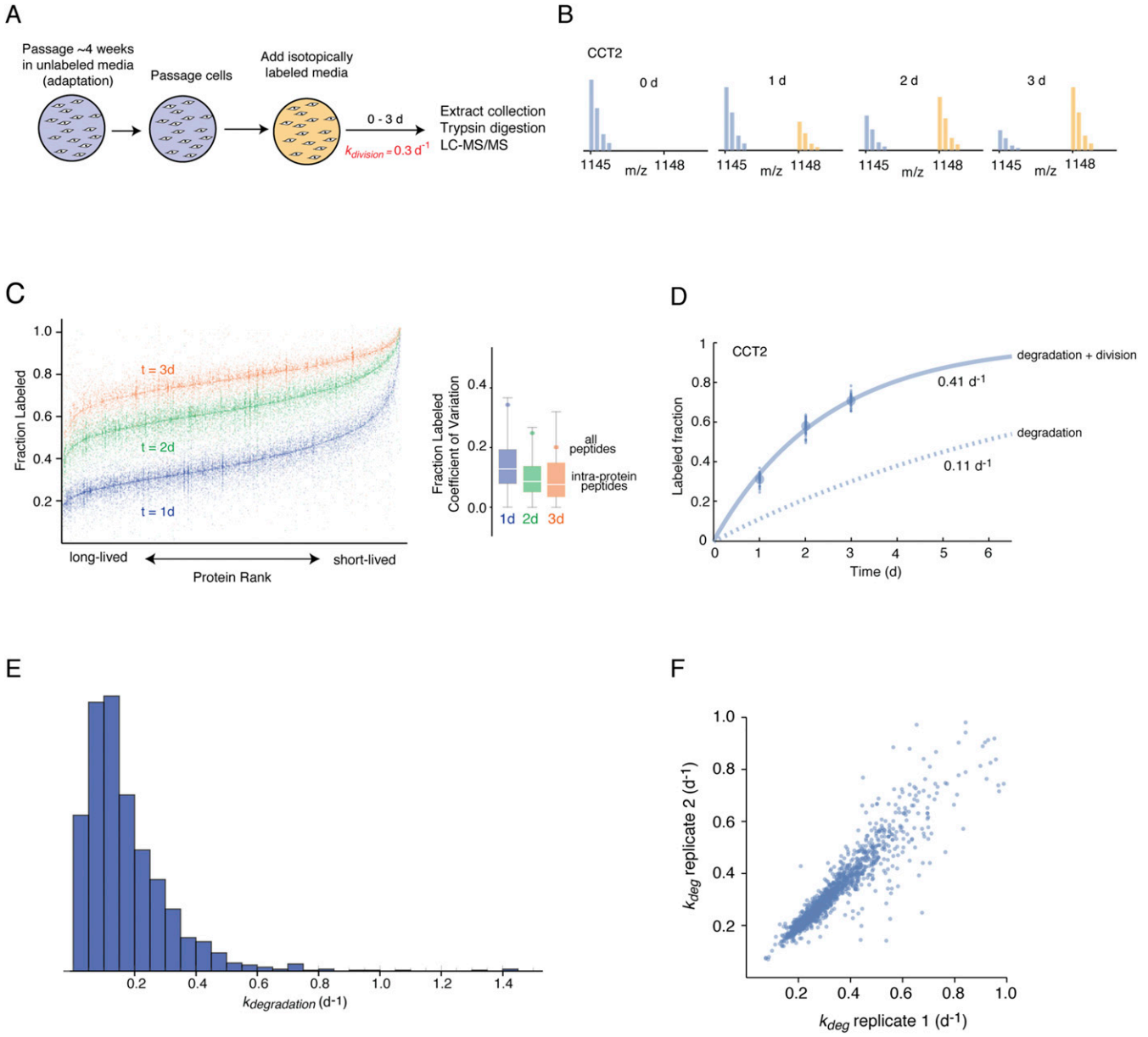

Fig. S1. Proteome-wide measurement of degradation rates in dividing fibroblasts. (*A*) Experimental design of dynamic SILAC experiments. (*B*) Example spectra showing the time-dependent labeling of a peptide mapped to CCT2. Blue and orange peaks indicate the unlabeled and labeled peptides, respectively. (*C*) Rank–size distribution plots showing the fractional labeling of peptides matched to each protein within the proteome at different time points for dividing fibroblasts. Note that the range of measured fractional labeling for peptides within each protein is significantly narrower than the entire range of measured peptides. The box plots indicate the range of coefficient of variations (CVs) for measured fractional labeling of peptides mapped to the same protein. The dots indicate the CV for all peptides at a given time point. (*D*) Labeling kinetics of CCT2. Small dots indicate all peptides mapped to the protein, and the large dots indicated the median of all peptides. The lines are fits to exponential equations based on the model described in *Materials and Methods*. The dotted line indicates the theoretical degradation kinetics of the protein after subtraction of the division rate from the total clearance rate. (*E*) The distribution of $k_{degradation}$ measurements in dividing cells. (*F*) Biologically replicate measurements of $k_{degradation}$, indicating the precision of experiments.

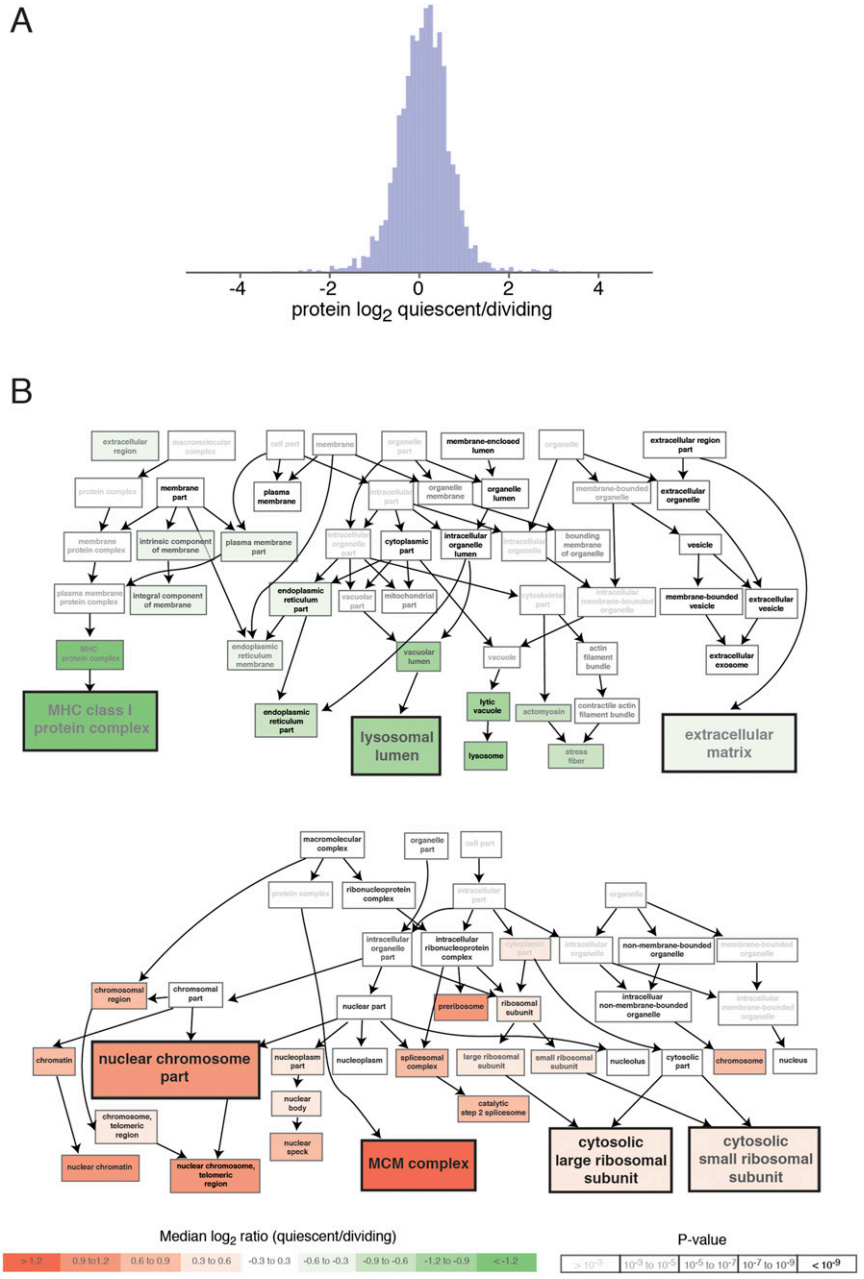

Fig. S2. Changes in steady-state protein expression levels between dividing and quiescent fibroblasts. (*A*) The distribution of log2 ratios of steady-state protein levels between quiescent and dividing cells. (*B*) Hierarchical gene ontology (GO) analysis of the up-regulation (green) and down-regulation (red) of protein levels. The statistical significance (*P* value) of gene enrichment of differentially expressed genes within each GO accession is indicated by boldness of font. The color shade indicates the median of log2 ratios (quiescent/dividing) of genes mapped to each accession. The hierarchical relationship between accessions is indicated by arrows. The analysis was conducted using the algorithms GOrilla and REViGO (see *Materials and Methods*). This figure is limited to the component GO category. The complete results of the GO analysis are tabulated in Dataset S4.

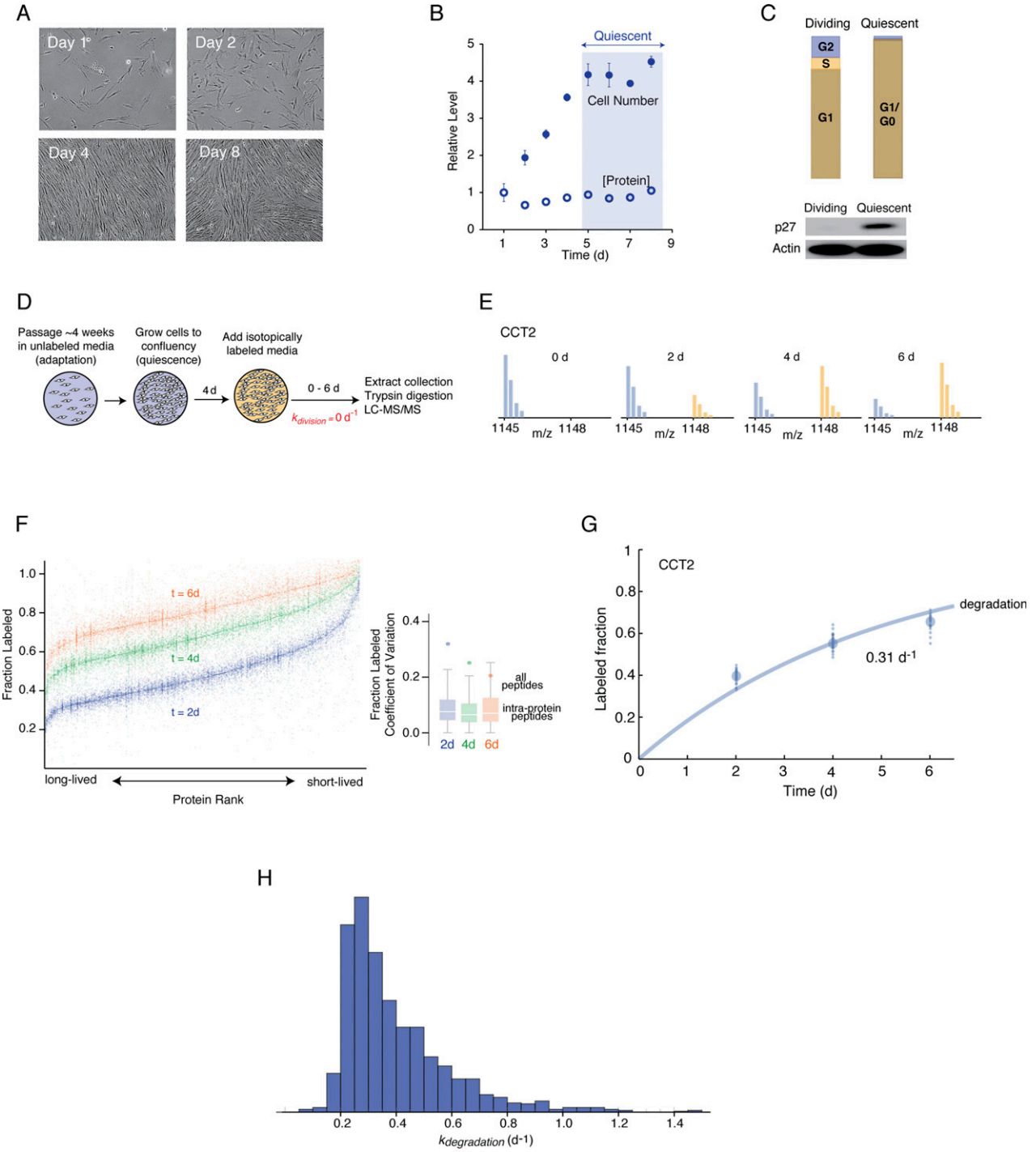

Fig. S3. Proteome-wide measurement of degradation rates in quiescent fibroblasts. (*A*) The transition of fibroblasts from a dividing to a contact-inhibited quiescent state. (*B*) Upon quiescence, [protein] per cell remains approximately constant despite the absence of cytoplasmic dilution by cell division. (*C*) FACS analysis of DNA content indicates that contact-inhibited fibroblasts are primarily in a G1/G0 state. The quiescent status of cells was verified by Western blot showing the up-regulation of the quiescence marker p27 in contact-inhibited cells. (*D*) Experimental design of dynamic SILAC experiments for measurement of degradation rates in quiescent cells. (*E*) Example spectra showing the time-dependent labeling of a peptide mapped to CCT2. (*F*) Rank–size distribution plots showing the fractional labeling of peptides mapped to different proteins. Refer to Fig. S1 for details. (*G*) Labeling kinetics of CCT2. Refer to Fig. S1 for details. (*H*) The distribution of $k_{degradation}$ measurements in quiescent cells.

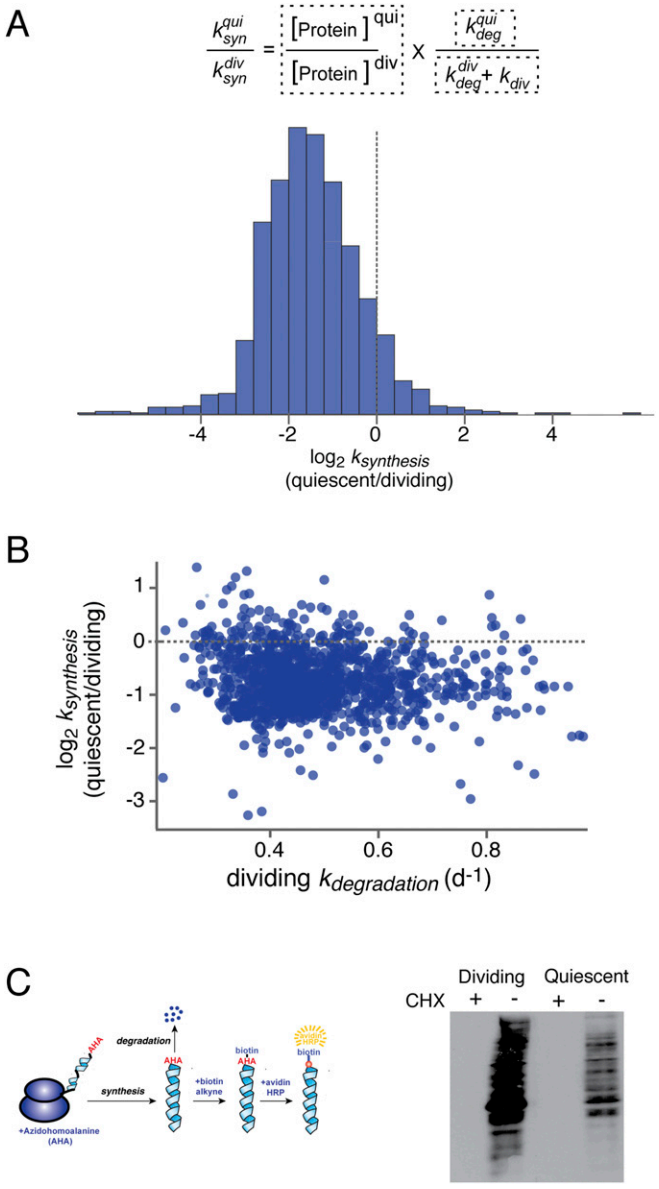

Fig. S4. Differences in protein synthesis between dividing and quiescent fibroblasts. (*A*) Distribution of $\log_2$ ratio of synthesis rates between quiescent and dividing cells. The ratios were determined according to the indicated equation and employing the three experimentally determined proteome-wide measurements (boxed). The analysis was based on the kinetic model described in *Materials and Methods*. (*B*) Scatter plot showing the relationship between $\log_2$ ratios of $k_{synthesis}$ measurements between quiescent and dividing cells and $k_{degradation}$ in dividing cells. The data indicate a uniform reduction in $k_{synthesis}$ for the entire proteome that is not correlated with protein stability. (*C*) Accumulation of newly synthesized proteins after 1 h of AHA labeling. The reduced accumulation of newly synthesized proteins in quiescent cells is consistent with a global reduction in $k_{synthesis}$. CHX indicates control experiments in the presence of the cycloheximide, an inhibitor of translational elongation.

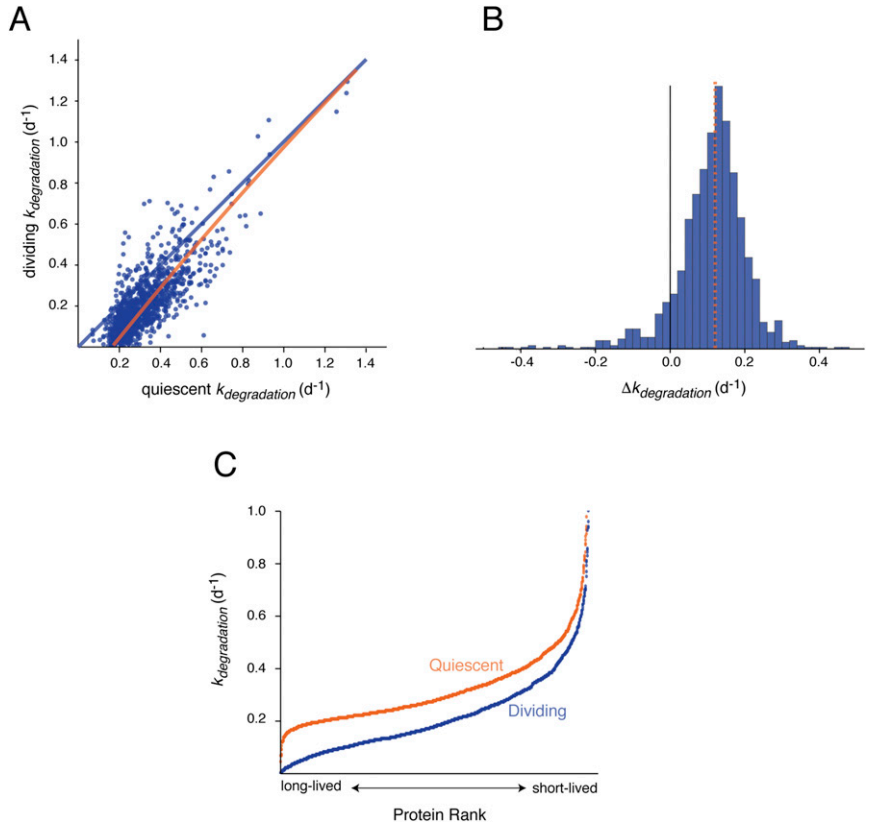

Fig. S5. Differences in protein $k_{degradation}$ between dividing and quiescent fibroblasts. (*A*) Pairwise comparison of $k_{degradation}$ measurements between quiescent and dividing cells. The blue line indicates the identity line, and the orange line indicates the best polynomial fit line to the data. (*B*) The distribution of differences in $k_{degradation}$ between quiescent and dividing cells ($\Delta k_{degradation}$). (*C*) Rank–size distribution plots of $k_{degradation}$ measurements in quiescent and dividing cells. Note that the differences in $k_{degradation}$ between the two states are significantly greater for long-lived proteins.

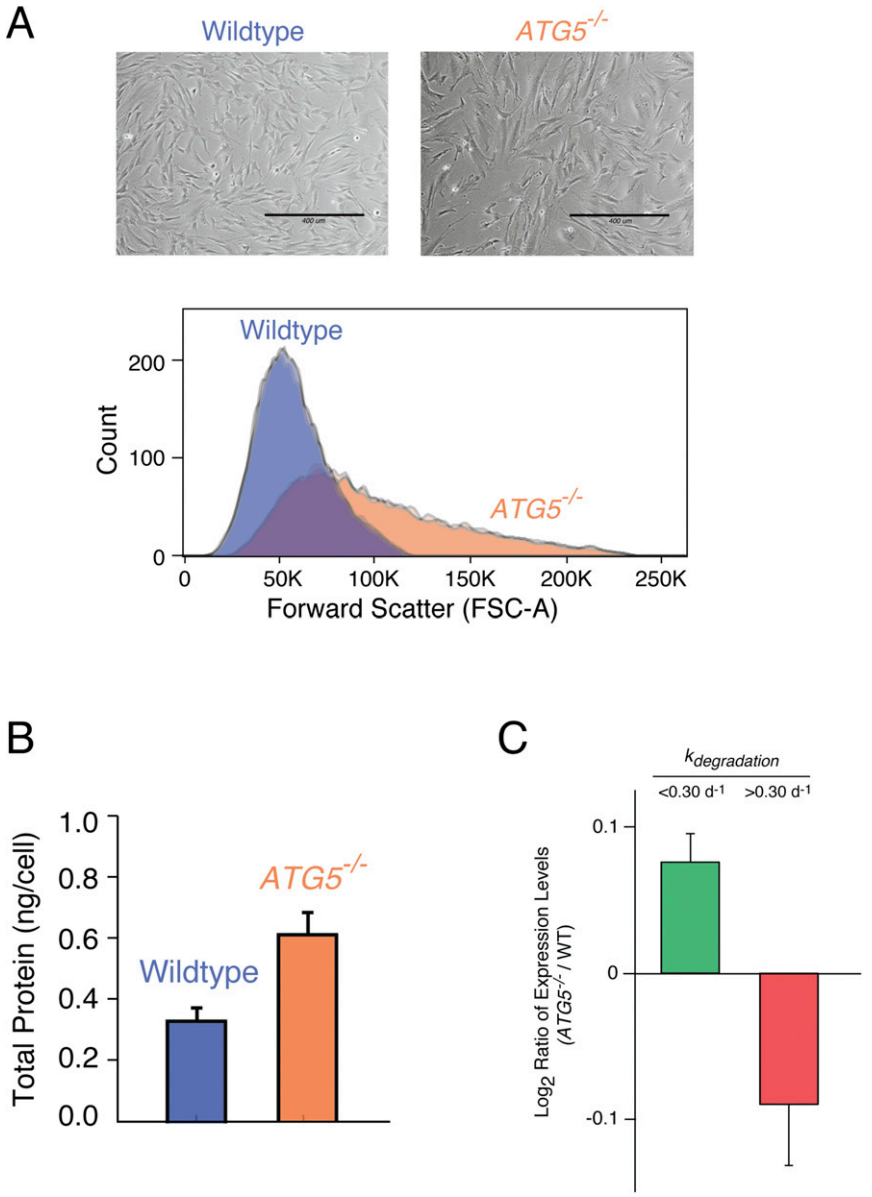

Fig. S6. Proteostatic phenotypes of ATG5$^{-/-}$ fibroblasts. (*A*) Quiescent ATG5$^{-/-}$ fibroblasts are characteristically larger than wild-type cells as indicated by microscopy and forward scatter intensity measurements by flow cytometry. (*B*) Quiescent ATG5$^{-/-}$ fibroblasts contain more total protein per cell as determined by BCA and cell count measurements. (*C*) SILAC experiments indicate that expression level of long-lived proteins are selectively increased in quiescent *ATG5*$^{-/-}$ cells (see ref. 9).

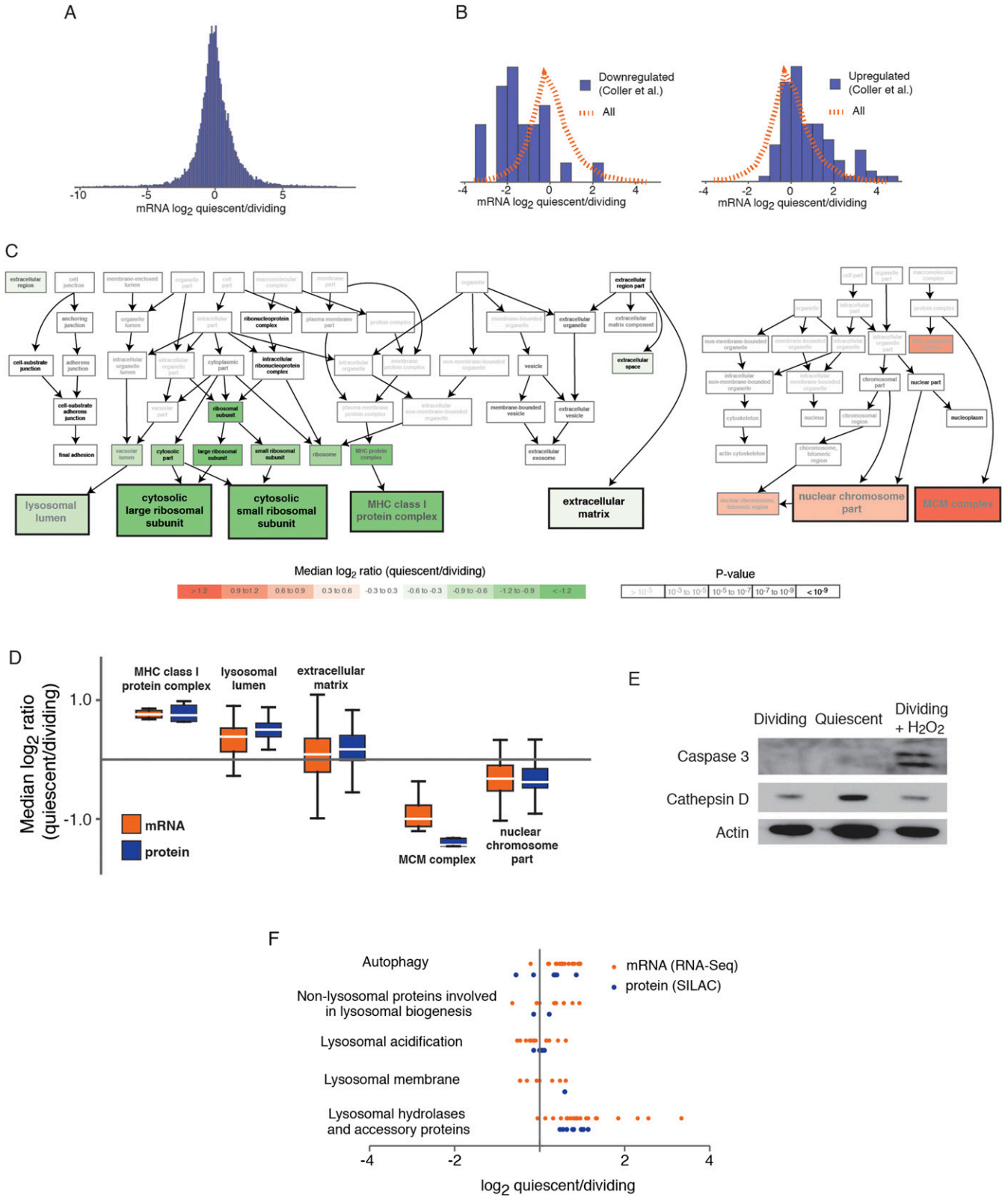

Fig. S7. Differences in steady-state mRNA and protein expression levels between dividing and quiescent fibroblasts indicate that lysosomal biogenesis is up-regulated in quiescent cells. (*A*) The distribution of log2 ratios of steady-state mRNA levels between quiescent and dividing cells. (*B*) The distribution of log2 ratios of steady-state mRNA levels between quiescent and dividing cells for genes shown by Coller et al. (5) to be differentially expressed. (*C*) Hierarchical gene ontology (GO) analysis of the up-regulation (green) and down-regulation (red) of mRNA levels. See Fig. S2 for additional details. (*D*) Box plots indicate the distribution of $\log_2$ ratios of mRNA and protein levels for each GO accession. The box indicates the IQR, and the line indicates the median. Far outliers (>1.5*IQR) were excluded. (*E*) Western blots showing that the lysosomal protease cathepsin D, but not caspase 3, is up-regulated in quiescent cells. The data indicate that cathepsin up-regulation is not due to the presence of apoptotic cells. H_2O_2 treated cells are included as a positive apoptosis control. (*F*) Quiescence-induced changes in mRNA and protein expression levels of lysosome-related proteins broken down by functional categories.

Dataset S1. Dynamic SILAC peptide and protein level data for dividing wild-type, quiescent wild-type, quiescent ATG5$^{-/-}$, dividing ATG5$^{-/-}$, quiescent PSME knockdown, and dividing PSME knockdown cells (related to Figs. 2 and 4)

Dataset S1

Dataset S2. Steady-state SILAC comparison between dividing and quiescent wild-type cells (related to Fig. 3)

Dataset S2

Dataset S3. Steady-state RNA-Seq comparison between dividing and quiescent wild-type cells, (related to Fig. 3)

Dataset S3

Dataset S4. GO analysis for steady-state SILAC and RNA-seq (related to Fig. 3)

Dataset S4